J Ind Microbiol Biotechnol (2010) 37:1023–1031
DOI 10.1007/s10295-010-0749-y

ORIGINAL PAPER

Large-scale production of magnetic nanoparticles using bacterial fermentation

Ji-Won Moon · Claudia J. Rawn · Adam J. Rondinone · Lonnie J. Love · Yul Roh · S. Michelle Everett · Robert J. Lauf · Tommy J. Phelps

Received: 4 May 2009 / Accepted: 20 May 2010 / Published online: 11 June 2010

Abstract Production of both nano-sized particles of crystalline pure phase magnetite and magnetite substituted with Co, Ni, Cr, Mn, Zn or the rare earths for some of the Fe has been demonstrated using microbial processes. This microbial production of magnetic nanoparticles can be achieved in large quantities and at low cost. In these experiments, over 1 kg (wet weight) of Zn-substituted magnetite (nominal composition of $Zn_{0.6}Fe_{2.4}O_4$) was recovered from 30 l fermentations. Transmission electron microscopy (TEM) was used to confirm that the extracellular magnetites exhibited good mono-dispersity. TEM results also showed a highly reproducible particle size and corroborated average crystallite size (ACS) of 13.1 ± 0.8 nm determined through X-ray diffraction ($N = 7$) at a 99% confidence level. Based on scale-up experiments performed using a 35-l reactor, the increase in ACS reproducibility may be attributed to a combination of factors including an increase of electron donor input, availability of divalent substitution metal ions and fewer ferrous ions in the case of substituted magnetite, and increased reactor volume overcoming differences in each batch. Commercial nanometer sized magnetite (25–50 nm) may cost $500/kg. However, microbial processes are potentially capable of producing 5–90 nm pure or substituted magnetites at a fraction of the cost of traditional chemical synthesis. While there are numerous approaches for the synthesis of nanoparticles, bacterial fermentation of magnetite or metal-substituted magnetite may represent an advantageous manufacturing technology with respect to yield, reproducibility and scalable synthesis with low costs at low energy input.

Keywords *Thermoanaerobacter* sp. TOR-39 · Fermentation · Mass production · Magnetite · Mono-dispersity · Reproducibility

J.-W. Moon · S. M. Everett · R. J. Lauf · T. J. Phelps (✉)
Biosciences Division, Oak Ridge National Laboratory, Oak Ridge, TN 37831, USA
e-mail: phelpstj@ornl.gov

C. J. Rawn
Materials Science and Technology Division, Oak Ridge National Laboratory, Oak Ridge, TN 37831, USA

A. J. Rondinone
Center for Nanophase Materials Sciences Division, Oak Ridge National Laboratory, Oak Ridge, TN 37831, USA

L. J. Love
Measurement Science and Systems Engineering Division, Oak Ridge National Laboratory, Oak Ridge, TN 37831, USA

Y. Roh
Faculty of Earth System and Environmental Sciences, Chonnam National University, Gwangju 500-757, Republic of Korea

Introduction

Recently, industrial demands for magnetic powders have increased as the number of potential applications for the material has grown. Magnetic nano-sized powder can be used as a medicine carrier for site-specific chemotherapy [38], magnetic storage devices [1], magnetocaloric pumps [12], ferrofluids [13], magnetic resonance imaging [9, 10] and radar absorbing materials [2]. Another possible application includes water purification [29, 33]. Considerable efforts to enhance the properties of magnetite (Fe_3O_4) have been pursued because magnetite does not have significant oxidation problems compared to zero valent iron nanoparticles. However, it is hard to cheaply mass produce

homogeneous magnetite between 5 and 50 nm [30]. Successful commercialization of the technology hinges on factors of quality, cost and availability.

Bacterial fermentation represents a fundamentally new approach for large-scale production of nanometer-sized crystalline powders of various materials. Previous work [12, 13] supported the development of high throughput synthesis of pure and metal substituted magnetite. Recent research with thermophiles indicated that the microbially mediated process is suitable for incorporating other metals into magnetite, including Co, Ni, Zn, Cr, Mn and Pd [15, 16, 23, 25, 26, 34] and rare earths such as Nd, Gd, Er, Ho and Tb [17]. The work presented here focuses on the development of a low cost approach to produce highly controlled magnetite nanoparticles having uniform size ranges within 5–100 nm in kg-sized batches. Figure 1 shows prototype scale-up experiments from 10-ml to 12-l volumes with bacterially synthesized metal-substituted nanoscale magnetite powders.

Bacterial fermentation for nanoscale magnetic powder synthesis has definite advantages in terms of scalability, reproducibility and high quality with low defects or dislocations compared to traditional inorganic methods such as sol-gel [32], chemical vapor decomposition [22] or magnetosome magnetite using magnetotactic bacteria [7]. Key aspects for mass production by bacterial fermentation include the rate at which particles are produced, size reproducibility and ease of recovery. As for ease of recovery, the final products can be recovered by washing with deionized water to remove the medium solution. In contrast, synthesis using organometallic precursors uses various kinds of solvents such as 1,2 hexadecanediol, oleylamine and oleic acid in phenyl ether [28] and 1-hexadecene, octyl ether, 1-octadecene, 1-eicosene and trioctylamine [19], which are harmful to the environment. Also, a surface treatment to transform hydrophobic surfaces of the nanoparticles to hydrophilic is essential in the inorganic synthesis. Another important advantage is the low temperature and low energy input compared to chemical syntheses using thermal decomposition [4, 5] and mechanical grinding to achieve the desired particle sizes [20].

Fig. 1 Prototype scale-up experiments from 10 ml, 100 ml, 500 ml, 1 l and 12 l of medium

The low temperatures and corresponding lower energy costs and high yield may make bacterial fermentation a more economical and energy sustainable process than some of the competing processes. For example, the synthesis using an organometallic complex requires at least 500°C to decompose the precursors [21], and synthesis using the sol-gel method needs annealing at least 250°C under vacuum [32], while microbial fermentation only needs temperatures between 20 and 65°C. The prices of commercial magnetite in 2009 US dollars generally exceed $500/kg (98%, <50 nm, Sigma-Aldrich or 99.5%, 25 nm, Nanostructured and Amorphous Materials), while microbial mass production is likely capable of producing 30 nm magnetite at a small fraction of the cost of traditional chemical synthesis.

Materials and methods

Source of microorganism, media preparation and incubation, and sample collection

Fe(III)-reducing bacteria (thermophilic, mesophilic or psychrotolerant strains) have been isolated from sediments and water collected from a variety of environments including deep subsurface sediments or hydrothermal vents in the ocean [11, 24, 27]. These Fe(III)-reducing bacteria are capable of synthesizing pure and metal-substituted magnetite nanoparticles under anaerobic conditions [14, 37]. *Thermoanaerobacter* sp. TOR-39 [11] was chosen to examine microbial formation of magnetite in larger scale production scenarios, because they enable crystalline reaction products to be obtained within days to weeks of incubation. Also 10 mM of potential electron donors such as glucose, lactate and acetate [11] for reduction of akaganeite form and synthesis of magnetite was tested by incubation with 80 mM of pure akaganeite and TOR-39 for 2 weeks. Samples with lactate and acetate showed magnetic black precipitates only on the surface of the precipitated precursor. In contrast, samples with glucose exhibited fully transformed magnetites (data not shown). Therefore, further syntheses used only glucose to intensify a high yield mass production.

The culture medium contained the same basal composition as previously reported [16]. No exogenous electron carrier substance (i.e., anthraquinone disulfonate) or reducing agent (i.e., cysteine) was added to the anaerobic medium.

To initiate the 35-l reactor (Fig. 2a), 20 l of condensed basal medium having ingredient equivalents to 30 l was added to a 25-l glass carboy, equipped with ventilation ports, and was autoclaved for 2 h. The carboy remained in the autoclave until the temperature decreased to 70°C. The carboy was further cooled with continuous purging using purified N_2 gas through a 0.2-μm filter overnight. Cooled medium was transferred by adding pressure (<0.25 atm) to the head space of the carboy, consequently transferring the medium to the sterilized 35-l reactor purged with N_2 gas. After the temperature of the medium in the reactor approached 65°C, the incubation for the mass production of pure or metal-substituted magnetites was initiated with the addition of 10 mM of glucose, 15 mM of 3-(N-morpholino)propanesulfonic acid (MOPS) titrated to a pH of 7.8, about 80–120 mM of akaganeite ($M_xFe_{1-x}OOH$, where M is metal) precursor and 2 l of mid-log growth TOR-39, which was prepared by fermenting without an electron acceptor at 65°C for 1 or 2 days using 2 volume % transfer from a stored culture. The total fermentation volume was adjusted to 30 l with anaerobic sterile distilled water. Injections were made using 18G needles, double male Luer Lock stainless steel fittings and N_2 gas sparging. Each 0.4 M pure and metal-substituted akaganeite as magnetite precursor was prepared [16] and aged at least 1 month prior to fermentation.

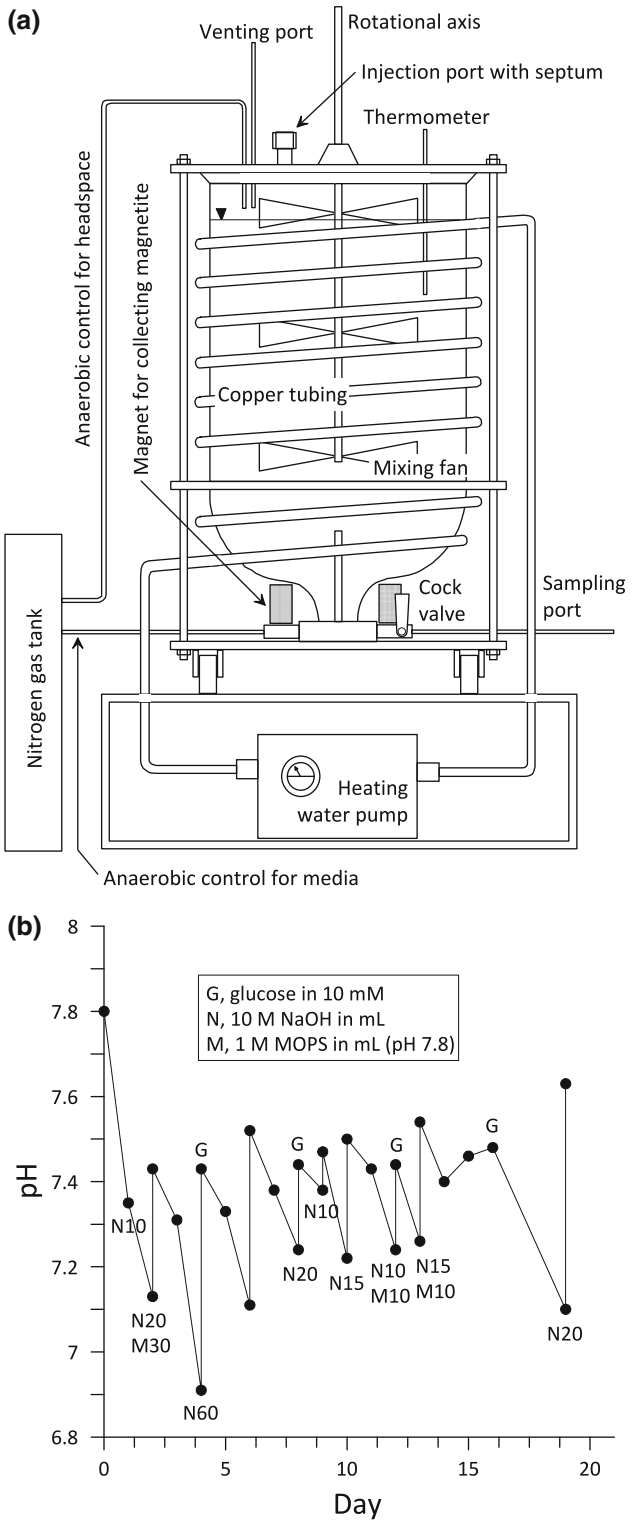

Fig. 2 **a** Schematic diagram of the 35-l reactor for large-scale fermentative production of nanoparticles (*upper*) and **b** operating the reactor with pH control

The incubation was maintained at 65°C for 3 weeks, and the medium was supplemented with 10 mM glucose every 4 days. The pH was measured on subsamples taken from the vessel using a combination of a pH electrode (Orion 815600) with an expandable ion analyzer (Orion EA-920, ThermoOrion, Beverly, MA; Fig. 2b). Aliquots of 10 M·NaOH or 1.5 M·MOPS were added as needed to maintain pH between 7.2 and 7.5. During the incubation, continuous purging with N_2 gas maintained anaerobic conditions of the media and removed CO_2 gas in the headspace through a back pressure valve (0.2 bar). This both assured the safety of the reactor and prevented carbonate precipitates. The contents of the reactor were stirred continuously at 40 rpm, and vigorous mixing was performed for more than 30 min every day.

Chemical and mineralogical characterization of magnetic nanoparticles

After the scheduled incubation time, subsamples in pressure tubes or serum bottles were collected as described previously [16]. Magnetite from the 35-l reactor was collected via a sampling port while keeping a positive headspace pressure by adding N_2 gas. Remaining in the reactor was approximately 10 l of used medium. New medium was subsequently added for the next fermentation batch. Solid mineral phases from the reactor were washed a minimum of five times by repeated cycles of vigorous stirring in 15 l of deionized water in a 20-l bucket and subsequent separation using two strong magnets (150 × 70 × 35 mm

each). Samples containing minimum water were degassed with N_2 for more than 1 h, weighed as wet samples and stored in glass bottles with a gas-tight seal under N_2 gas. Subsamples for analyses were extracted in the glove bag, freeze dried and then stored under N_2 gas.

For the X-ray powder diffraction characterization, a small amount of microbially produced nano-sized magnetite was mixed with methanol to make a slurry, and the slurry was applied to a silica zero background plate. Data were collected using either a Scintag PAD V with a Peltier cooled point detector or a PANalytical, X'pert PRO MPD diffractometer with a real-time multiple strip (RTMS) X'Celerator detector. Both instruments used Cu-kα radiation and were operated at a power of 45 kV/40 mA, and data were collected between 10 and 70° 2θ. Data were analyzed by profile fitting without any structural parameters using the JADE software package (Material Data Inc.) and/or fitting with structural parameters using the EXPGUI graphical user interface [31] for the General Structure Analysis System (GSAS) Rietveld program [8]. ACS was determined using the JADE software, and the Scherrer equation and lattice parameters were obtained from Rietveld refinements using GSAS.

Transmission electron microscopy (TEM, FX 2000, JEOL, Japan) was used to study the morphology and particle size of the precipitated iron minerals.

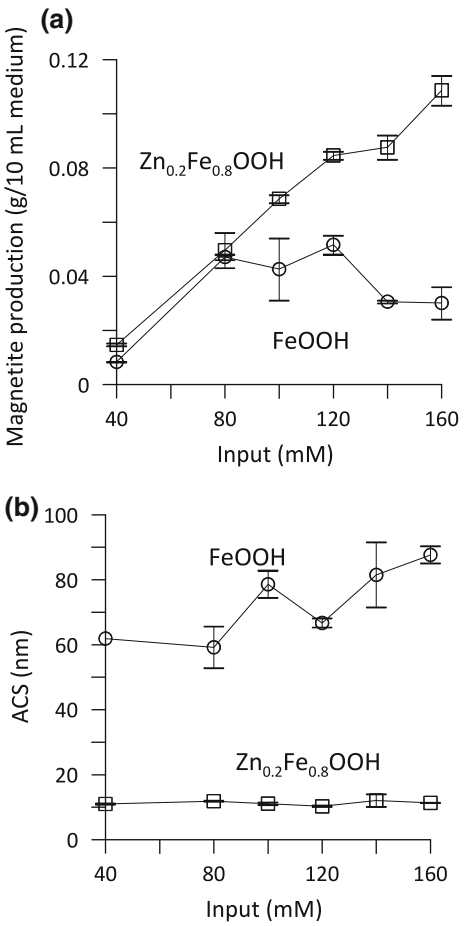

Fig. 3 Changes in production mass (**a**) and average crystallite size (ACS) (**b**) according to the input amounts of pure and Zn-substituted precursor from 40 to 160 mM in pressure tubes

Results and discussion

Effect of increased solutes (high input range 40–160 mM of magnetite precursor)

In previous studies either 40 mM [16, 17] or 70 mM of magnetite akaganeite precursor [23] was used in the pressure tubes. To possibly improve product yield, concentrations of pure precursor and Zn-substituted precursor were increased from 40 to 160 mM (Fig. 3). The effects of increasing the akaganeite precursor concentrations on product yields (Fig. 3a) and ACS (Fig. 3b) with 10 mM glucose as an electron donor were different between the pure precursor and Zn-substituted precursor ($Zn_{0.2}Fe_{0.8}OOH$). Increasing pure magnetite precursor concentrations may have decreased product sorption density thereby decreasing the yield, which is consistent with particle aggregation blocking Fe(II) sorption sites at higher solid concentrations [11]. In contrast, increasing the Zn-precursor concentration appeared to improve the product yield.

When using FeOOH as the precursor, the yield initially increased and then decreased at higher concentrations, while the ACS increased slightly with increasing precursor concentration. This result suggested that the microbial activity may not have sufficiently reduced ferric ions to generate enough magnetite nuclei, which then resulted in a larger ACS when the precursor concentration exceeded 80 mM. The low concentration of electron donor (relative to the increased amounts of precursor) and weak microbial activity predominantly facilitated crystal growth, as small nanoparticles were largely unobserved.

For the Zn substituted precursor ($Zn_{0.2}Fe_{0.8}OOH$), the yield of Zn-substituted magnetite (nominal formula $Zn_{0.6}Fe_{2.4}O_4$) increased, and the ACS was relatively stable with increasing precursor input. The Zn-substituted precursor series had available divalent Zn ions with additional reduced ferrous ions, so that a larger amount of Zn-substituted magnetite, in proportion to the input amount, could be produced during the 3-week fermentation and aging process even under constrained electron donor conditions. The stable ACS might be due to the balance between nuclei generation and crystal growth, and the size may have been controlled by the doping element [18]. They revealed that the formation of biomagnetite between nuclei generation and consumption by crystal growth was likely affected by

different doping metals followed by different metal-specific toxicity to bacteria, different hydrolysis constant of metals in precursors and incongruent incorporation of different dissolved metal species in the media.

Effect of medium scale-up (low input range 20 and 40 mM of magnetite precursor)

The scale-up of the reaction vessel appeared to have a positive influence on ACS. With the addition of either 20 or 40 mM of pure magnetite precursor into 10, 50, 200 (or 500), and 1,000 ml media, a general trend was noted: the larger the medium volume, the smaller the crystallite size (Fig. 4a). The trend may be related to the increased precursor input volume per unit area as precursors typically settled to the vessel bottom after the inoculation, where precipitation ensued in the condensed state (henceforth termed condensed density). The larger condensed densities occurred at the larger media volumes resulting in smaller particle sizes. These observations were in agreement with the results of Casula et al. [3] who noted that the concentration of the iron precursor affected the size of the resulting nanoparticles in such a way that smaller particles were obtained at higher iron concentrations. Therefore, the effect of medium volume was likely related to the heterogeneous (condensed) distribution of precursor and not to the ideal homogeneous distribution of precursors in the total medium volume. We also tested the formation of biomagnetite with continuous stirring at 120 rpm in duplicate or triplicate. Both 20 and 40 mM input samples with stirring exhibited a similar trend with stagnant samples except the 10-ml scale. Under stirring conditions, diffusion and aggregation of magnetite monomers were expected to be enhanced, and the quantity of the micelle aggregates increased [35], causing increased ACS. However, biomagnetite formation resulted in little difference. Large variation at the 10-ml scale samples can be interpreted by the ratio of bottom area and medium volume (Fig. 4b). The ratio was very close among 50, 200 and 1,000 ml ($r^2 = 0.9991$). When 10- and 500-ml volumes were included, there was a poorer correlation ($r^2 = 0.9633$).

Our observation of larger ACS with 40 mM of precursor than with 20 mM precursor over the entire range of media volumes (Fig. 4a) seems at odds with the above interpretation of smaller ACS with larger media volume or ion concentration. A larger ACS trend at 40 versus 20 mM of akaganeite precursors suggests that crystal growth may have dominated over nuclei formation, when the precursor input was low. Accordingly, the larger ACS between our 40 versus 20 mM experiments should not be directly contrasted with the smaller ACS observations at the much higher range of 100–300 mM precursors discussed by Casula et al. [3]. The difference of ACS between 40 and 20 mM precursor input concentration diminished with increasing medium volume when the electron donor condition was unconstrained. Moon et al. [16] previously used X-ray powder diffraction to determine that the 10 mM of glucose used was sufficient for the transformation of 40 mM precursor. Under the conditions presented here (different input precursor concentrations and sufficient electron donors), the similar ACS at larger medium volumes indicated that size control and mono-dispersivity of microbial synthesis was consistent in larger scale reactors. The consistency was likely due to sustained microbial activity at the higher volumes resulting in faster and continuous nuclei generation.

The results presented here and in the literature indicate that ACS is likely controlled by a combination of input concentration range, precursor type and condensed density with respect to volume. The formation of more magnetite

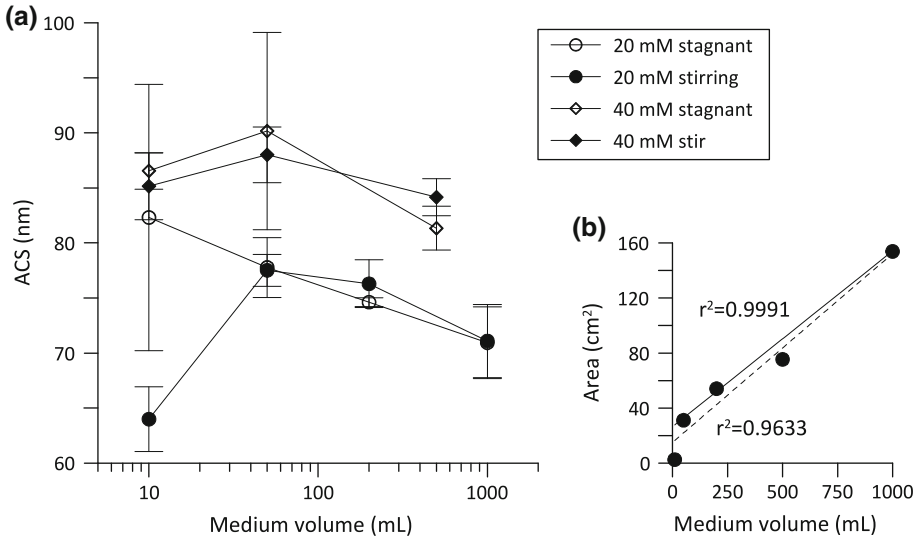

Fig. 4 **a** Crystallite size depending on medium volume, precursor input concentration and stirring during the production of pure magnetite; **b** correlation between bottom area and medium volume

nuclei typically resulted in smaller ACS because of the interrelationship between nanocrystal nucleation and nanoparticle growth [36].

There are contrasting forces that may control ACS in these experiments. Considering the relationship between Ostwald ripening and electron donors, one possibility could be that ACS would be proportional to input concentration of electron acceptors (Fig. 3b) where smaller nanoparticles dissolve and deposit onto the larger nanoparticles [6]. Another possibility could suggest an ACS inversely proportional to the condensed density with unconstrained electron donors slowing the growth of larger particles and accelerating the growth of smaller ones, resulting in a narrow size distribution (Fig. 4) of nanoparticles. This increase of ACS could be suppressed by the dissolved iron concentration being close to supersaturation based on increased condensed densities. For large-scale microbial production of magnetite starting with akaganeite precursors, the growth of nanoparticles may be controlled by an excess of precursor, increasing the condensed densities of precursors with unconstrained electron donors and facilitating nucleation followed by the accumulation of small-sized nanoparticles.

Scale-up experiment and reproducibility

Table 1 shows scale-up experiment results, up to 30 l, producing pure and metal-substituted magnetites. A 30-l batch fermentor can yield over 1 kg (wet weight) of magnetite in less than 1 month as opposed to magnetotactic bacteria synthesis, which may yield only a few grams for the same volume and incubation time. Compared to pure magnetite of 41.3 ± 5.1 nm from a 30-ml medium scale [34], 30-l fermentation produced pure magnetite of 75.8 ± 5.1 nm ACS. The greater ACS of pure magnetite in the 30-l experiments was in a good agreement with the mechanism suggesting that lower production of nuclei leads to larger particle size (Fig. 3b). In contrast, the ACS of various metal-substituted magnetites in the large-scale (30-l) experiments was smaller than that from small-volume cultures such as $Zn_{0.3}Fe_{2.7}O_4$ (37.0 ± 3.3 nm from 50 ml and 28.4 ± <0.1 nm from 30 l) and $Co_{0.3}Fe_{2.7}O_4$ (47.7 ± 11.5 nm from 50 ml and 33.9 ± 3.1 nm from 30 l). This implies that upscaled microbial synthesis provided advantages of yield and mono-dispersive crystallite control atypical of chemical nanoparticle synthesis providing smaller ACS for substituted magnetite that might be due to the additional supply of divalent cations.

A complication was that the samples prepared in 1 l of medium have relatively large estimated standard deviations of ACS compared to 50-ml culture volumes or 30-l batch fermentations (data not shown). This may have been an experimental artifact because of the different initial conditions with separately prepared media for each bottle (the 1 l experiments) in contrast to medium from a single large batch (the 50 ml bottles) or a large medium volume (30 l), which minimized deviations during medium preparation. A different phenomenon was likely responsible for the larger standard deviations of the ACS of nanoparticles incorporating Ni and Co than for ACS of pure and Zn-substituted magnetite nanoparticles. These differences were most likely due to differences in hydrolysis constants as Zn is closer to that of Fe than those of Ni and Co [15, 16]. The large standard deviations on the magnetite ACS produced from 1 l of medium volumes underscore the importance of controlling the initial conditions of lag time, dissolution of precursor and nucleation growth.

Repeated upscale 30-l fermentations (35-l reactor) using a single batch of media after repeated additions of electron donor and inoculation of the thermophilic TOR-39 culture with Zn-substituted precursor varying from 80 to 120 mM

Table 1 Production of various pure and substituted magnetites

Doping elements	Nanoparticle formula	Input concentration (mM)	Average crystallite size (nm)	Maximum yield (g/l)
Fe only[a]	Fe_3O_4	107	75.8 ± 5.1	19.6[b]
Zn[a]	$Zn_{0.6}Fe_{2.4}O_4$	80–120	13.0 ± 0.8	49.7[b]
Zn[a]	$Zn_{0.3}Fe_{2.7}O_4$	107	28.4 ± <0.1	23.5[b]
Co[a]	$Co_{0.3}Fe_{2.7}O_4$	107	33.9 ± 3.1	32.5[b]
Ni[a]	$Ni_{0.3}Fe_{2.7}O_4$	107	35.7 ± 5.6	24.4[b]
Mn	$Mn_{0.6}Fe_{2.4}O_4$	80	18	4.5[b]
Cr	$Cr_{0.15}Fe_{2.85}O_4$	40	40	0.85[c]
Nd	$Nd_{0.06}Fe_{2.94}O_4$	40	14	1.1[c]
Gd	$Gd_{0.06}Fe_{2.94}O_4$	40	23	1.2[c]
Ho	$Ho_{0.06}Fe_{2.94}O_4$	40	30	1.1[c]
Er	$Er_{0.06}Fe_{2.94}O_4$	40	32	0.9[c]
Tb	$Tb_{0.06}Fe_{2.94}O_4$	40	36	1.0[c]

[a] From 30-l medium volume and others from less than 1-l medium volume

[b] Wet weight with minimum water

[c] Dry weight

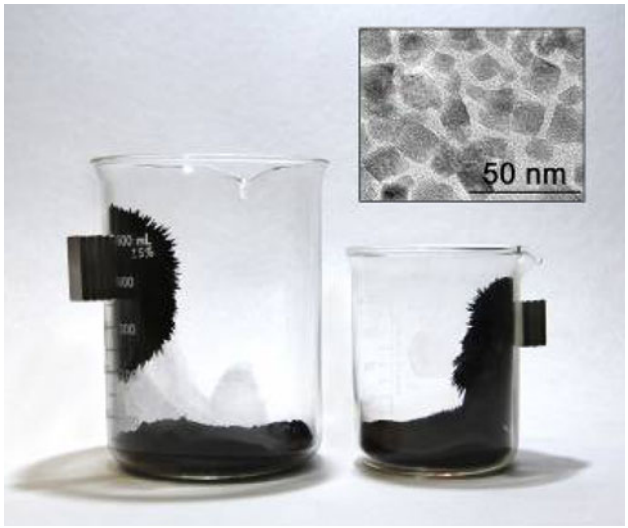

Fig. 5 Photograph of pure magnetite (Fe_3O_4, *left*) and Zn-substituted magnetite ($Zn_{0.6}Fe_{2.4}O_4$, *right*). Inset is TEM image of Zn-substituted magnetite

(by adding 6–9 l of 0.4 M $Zn_{0.2}Fe_{0.8}OOH$ into a final 30-l volume) produced up to 50 g/l (wet based) of Zn-substituted magnetite (Fig. 5). TEM imaging after the particle separation procedure (inlet of Fig. 5) exhibited average long and short axes of 15.4 and 12.9 nm ($N = 27$). Various doping elements and different precursor input concentrations were examined with additional electron donor and pH control at 7.3–7.5, and results are presented from the Zn-substituted system (Fig. 6). Two subsamples (nos. 7 and 8) were out of the statistical lower and upper bounds of 11.5- and 14.6-nm ACS at the 99% confidence level and were excluded from subsequent analysis. TEM microphotographs of Zn-substituted magnetites exhibited a good mono-dispersivity (Fig. 6a, b). The ACS from the X-ray diffraction patterns exhibited a high reproducibility of 13.1 ± 0.8 (1σ) nm based on seven samples and a good agreement with the TEM result. Seven of nine consecutive fermentation batches exhibited remarkably similar values for the lattice parameter (Fig. 6c), indicating excellent reproducibility. The lattice parameters converged to a narrow range from 8.411 to 8.416 Å with the average lattice parameter of 8.413 ± 0.002 Å (except no. 7 of 8.421 Å beyond the upper bound at 99% confidence level; Fig. 6c). After the seventh batch, all of the media was flushed from the vessel, and the reactor was filled with new media because of an accumulation of volatile fatty acids that presumably was associated with a larger lattice parameter with a larger standard deviation than the previous batches. Again, the final two batches exhibited similar lattice parameters to the first six (Fig. 6c).

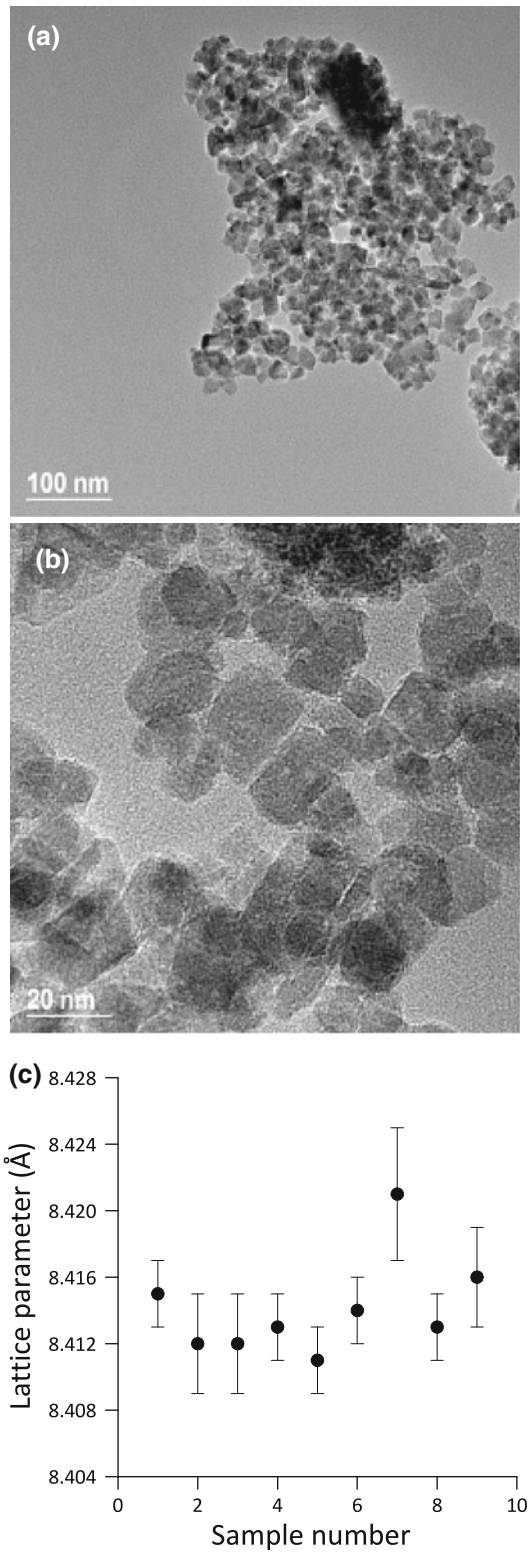

Fig. 6 **a** and **b** TEM images of Zn-ferrite from the 35-l reactor incubated at 65°C for 3 weeks. **c** Reproducibility examination as lattice parameter

The ACS of the 30-l fermentation batches exhibited good reproducibility of 13.1 ± 0.8 nm, even though precursor input concentrations ranged from 80 to 120 mM (Fig. 6). Generally, input concentration and medium volume affected the ACS of the resulting nanoparticles in such a way that smaller particles were obtained at higher condensed density during the microbial synthesis of magnetites. This is in agreement with results of chemical synthesis where a large supersaturation of solute resulted in more particles of smaller size [3, 21], which were assisted by organics or surfactants. Here, bacterial fermentation using the inoculation up to 120 mM precursor at a 30-l volume scale without aid of surfactants exhibited monodispersivity with reproducible and small ACS for the metal-substituted magnetites with shorter incubation time leading to advantageous upscaling of microbial nanoparticle production for the pure magnetite.

The control of ACS during both microbial and chemical synthesis was acquired by the competition between nucleation and growth. However, a short burst of nucleation followed by slow controlled growth appeared important to produce mono-dispersive particles in a chemical synthesis [6]. In contrast, microbially facilitated magnetite formation was found to produce mono-dispersive nanoparticles without delicate nucleation and growth control. Upscaling the microbial synthesis of magnetite and metal-substituted magnetites appears to have advantages of uniformity and reproducibility without complicated control processes.

Acknowledgments This research was supported by the Defense Advanced Research Projects Agency (DARPA) Biomagnetics Program under contract 1868-HH43-X1 and the US Department of Energy's (DOE) Office of Fossil Energy with student support provided by the DOE Environmental Molecular Science Initiative and US DOE's Office of Science, Biological and Environmental Research, Environmental Remediation Sciences Program (ERSP). ORNL is managed by UT-Battelle, LLC, for the US DOE under contract DE-AC05-00OR22725. J.-W. Moon was supported by an appointment to the ORNL Postdoctoral Research Associates Program administered jointly by the Oak Ridge Institute for Science and Education and ORNL.

References

1. Billas IML, Chatelain A, de Heer WA (1994) Magnetism from the atom to the bulk in nickel, cobalt and iron clusters. Science 265:1682–1684
2. Caffarena VDR, Ogasawara T, Pinho MS, Capitaneo JL (2007) Synthesis, characterization of nanocrystalline $Ba_3Co_{0.9}Cu_{1.1}Fe_{24}O_{41}$ powder and its application in the radar cross section reduction. Mat Sci Pol 25:875–884
3. Casula MF, Jun Y, Zaziski DJ, Chan EM, Corrias A, Alivisatos AP (2006) The concept of delayed nucleation in nanocrystals growth demonstrated for the case of iron oxide nanodisks. J Am Chem Soc 128:1675–1682
4. Goya GF, Berquó TS, Fonseca FC, Morales MP (2003) Static and dynamic magnetic properties of spherical magnetite nanoparticles. J Appl Phys 94:3520–3528
5. Gržeta B, Ristić M, Nowik L, Musić S (2002) Formation of nanocrystalline magnetite by thermal decomposition of iron choline citrate. J Alloys Compd 334:304–312
6. Hyeon T (2003) Chemical synthesis of magnetic nanoparticles. Chem Commun 8:927–934
7. Lang C, Schuler D (2006) Biogenic nanoparticles: production, characterization, and application of bacterial magnetosomes. J Phys Condens Mat 18:S2815–S2828
8. Larson AC, von Dreele RB (2000) General structure analysis system. Report LAUR. Los Alamos National Laboratory, Los Alamos, NM 86-748
9. Lee J-H, Huh Y-M, Jun Y-W, Seo J-W, Jang J-T, Song H-T, Kim S, Cho E-J, Yoon H-G, Suh J-S, Cheon J (2007) Artificially engineered magnetic nanoparticles for ultra-sensitive molecular imaging. Nat Med 13:95–99
10. Lemke A-J, Senfft von Pilsach M-I, Lübbe A, Bergermann C, Riess H, Felix R (2004) MRI after magnetic drug targeting in patients with advanced solid malignant tumors. Eur Radiol 14:1949–1955
11. Liu S, Zhou J, Zhang C, Cole DR, Gajdarziska M, Phelps TJ (1997) Thermophilic Fe(III)-reducing bacteria from the deep subsurface: the evolutionary implication. Science 277:1106–1109
12. Love LJ, Jansen JF, McKnight TE, Roh Y, Phelps TJ (2004) A magnetocaloric pump for microfluidic application. IEEE T Nanobiosci 3:101–110
13. Love LJ, Jansen JF, McKnight TE, Roh Y, Phelps TJ, Yeary LW, Cunningham GT (2005) Ferrofluid field induced flow for microfluidic application. IEEE T Mechatron 10:68–76
14. Lovley DR, Stolz JF, Nord GL Jr, Phillips EJP (1987) Anaerobic production of magnetite by dissimilatory iron-reducing microorganism. Nature 330:252–254
15. Moon J-W, Yeary LW, Rondinone AJ, Rawn CJ, Kirkham MJ, Roh Y, Love LJ, Phelps TJ (2007) Magnetic response of microbially synthesized transition metal- and lanthanide-substituted nano-sized magnetites. J Magn Magn Mater 313:283–292
16. Moon J-W, Roh Y, Lauf RJ, Vali H, Yeary LW, Phelps TJ (2007) Microbial preparation of metal-substituted magnetite nanoparticles. J Microbiol Methods 70:150–158
17. Moon J-W, Roh Y, Yeary LW, Lauf RJ, Rawn CJ, Love LJ, Phelps TJ (2007) Microbial formation of lanthanide-substituted magnetite by *Thermoanaerobacter* sp. TOR-39. Extremophiles 11:859–867
18. Moon J-W, Rawn CJ, Rondinone AJ, Yeary LW, Kirkham MJ, Wang W, Gu B, Phelps TJ (2010) Crystallite sizes and lattice parameters of nano-biomagnetite particles. J Nanosci Nanotechnol (in press)
19. Park J, An K, Hwang Y, Park J-G, Noh H-J, Kim J-Y, Park J-H, Hwang N-M, Hyeon T (2004) Ultra-large-scale syntheses of monodisperse nanocrystals. Nat Mat 3:891–895
20. Rabanal ME, Várez A, Levenfeld B, Torralba JM (2003) Optimization of the synthesis of soft magnetic materials by mechanochemical process at room temperature. Mater Sci Forum 424:4349–4354
21. Roca AG, Morale MP, Serna CJ (2006) Synthesis of monodispersed magnetic particles from different organometallic precursors. IEEE T Magn 42:3025–3029
22. Rogalski MS, Besserguenev V, Barata NRA, Baltazar R (2003) CVD synthesis and CEMS study of Fe sulfide and oxide thin film. IEEE T Magn 39:2696–2698
23. Roh Y, Lauf RJ, McMillan AD, Zhang C, Rawn CJ, Bai J, Phelps TJ (2001) Microbial synthesis and characterization of metal-substituted magnetites. Solid State Commun 118:529–534

24. Roh Y, Liu SV, Li G, Huang S, Phelps TJ, Zhou J (2002) Isolation and characterization of metal-reducing *Thermoanaerobacter* strains from deep subsurface environments of the Piceance Basin, Colorado. Appl Environ Microbiol 68:6013–6020
25. Roh Y, Zhang C-L, Vali H, Lauf RJ, Zhou J, Phelps TJ (2003) Biogeochemical and environmental factors in Fe biomineralization: magnetite and siderite formation. Clays Clay Miner 51:83–95
26. Roh Y, Vali H, Moon J-W, Phelps TJ (2006) Extracellular synthesis of magnetite and metal-substituted magnetite nanoparticles. J Nanosci Nanotechnol 6:3517–3520
27. Stapleton RD, Sabree ZL, Palumbo AV, Moyer CL, Devol AH, Roh Y, Zhou J (2005) Metal reduction at cold temperature by *Shewanella* isolates from various marine environments. Aqua Microbiol Ecol 38:81–91
28. Sun S, Zeng H, Robinson DB, Raoux S, Rice M, Wang SX, Li GJ (2004) Monodisperse MFe_2O_4 (M=Fe, Co, Mn) nanoparticles. J Am Chem Soc 126:273–279
29. Takeda S, Nishijima S (2006) The development of new magnet carrier method for the waste water treatment by the magnetic separation method. Chem Eng 51:614–619
30. Tartaj P (2006) Nanomagnets: from fundamental physics to biomedicine. Curr Nanosci 2:43–53
31. Toby BH (2001) EXPGUI, a graphical user interface for GSAS. J Appl Cryst 34:210–213
32. Xu J, Yang H, Fu W, Du K, Sui Y, Chen J, Zeng Y, Li M, Zou G (2007) Preparation and magnetic properties of magnetite nanoparticles by sol-gel method. J Magn Magn Mater 309:307–311
33. Yavuz CT, Mayo JT, Yu WW, Prakash A, Falkner JC, Yean S, Cong L, Shipley HJ, Kan A, Tomson M, Natelson D, Colvin VL (2006) Low-field magnetic separation of monodisperse Fe_3O_4 nanocrystals. Science 314:964–967
34. Yeary LW, Moon J-W, Love LJ, Thompson JR, Rawn CJ, Phelps TJ (2005) Magnetic properties of biosynthesized magnetic nanoparticles. IEEE T Magn 41:4384–4389
35. Yao S, Han Y, Liu W, Zhang W, Wang H (2007) Synthesis of CdS nanocrystals with different morphologies via an ultraviolet irradiation route. Mater Chem Phys 101:247–250
36. Yu WW, Peng X (2002) Formation of high-quality CdS and other II–IV semiconductor nanocrystals in noncoordinating solvents: tunable reactivity of monomers. Angew Chem Int Ed 14:2368–2371
37. Zhang C, Vali H, Romanek CS, Phelps TJ, Liu SV (1998) Formation of single-domain magnetite by a thermophilic bacterium. Am Miner 83:1409–1418
38. Ziolo RF, Giannelis EP, Weinstein BA, O'Horo MP, Ganguly BN, Mehrotra V, Russell MW, Huffman DR (1992) Matrix-mediated synthesis of nanocrystalline—γFe_2O_3: a new optically transparent magnetic material. Science 257:219–223